DOI: 10.1021/ma100920u

Macromolecules
ARTICLE

Surface Stress Effects on the Bending Direction and Twisting Chirality of Lamellar Crystals of Chiral Polymer

Hai-Mu Ye,[†] Jian-Shan Wang,[‡,#] Shuo Tang,[†] Jun Xu,[*,†] Xi-Qiao Feng,[*,‡] Bao-Hua Guo,[†] Xu-Ming Xie,[†] Jian-Jun Zhou,[§,&] Lin Li,[§,&] Qiong Wu,[⊥] and Guo-Qiang Chen[⊥]

[†]*Institute of Polymer Science & Engineering, Department of Chemical Engineering, School of Materials Science and Technology, Tsinghua University, Beijing 100084, China,* [‡]*Institute of Biomechanics and Medical Engineering, Department of Engineering Mechanics, Tsinghua University, Beijing 100084, China,* [§]*State Key Laboratory of Polymer Physics and Chemistry, Institute of Chemistry, Chinese Academy of Sciences, Beijing 100080, China, and* [⊥]*Department of Biological Sciences & Biotechnology, Tsinghua University, Beijing 100084, China.* [#]*Present address: Department of Mechanics, Tianjin University, Tianjin 300072, China.* [&]*Present address: College of Chemistry, Beijing Normal University, Beijing 100875, China.*

Received April 28, 2010; Revised Manuscript Received June 6, 2010

ABSTRACT: Expression of chirality in the highly ordered assembly structures of various types of natural and synthetic materials is still a mystery. Although surface stresses have been known to widely exist in polymer lamellae, how they affect the twisting chirality is yet an unsolved issue. Here we report inversion of the lamellar twisting chirality of microbial poly(*R*-3-hydroxybutyrate) copolymers from left-handed to right-handed via copolymerization or blending, with the molecular chirality and the structures in the crystalline core unchanged. We interpret the observed inversion of twisting chirality and the complicated lamellar curvature with a continuum model based on surface elasticity theory. Quantitative simulations reveal that the distribution of the anisotropic surface stresses and the surface elasticity property of the lamellae significantly affect the morphological chirality of lamellar twisting. For different chiral polymers, the same bending direction may correlate to the opposite twisting chirality.

Introduction

Chirality has been widely observed in the assemblies of inorganic materials,[1,2] organic materials,[3] and more complicated biological systems, e.g., DNA, RNA, and proteins at nano scale,[4] twisting polymer lamellar crystals at micro scale,[5] twisting flower petals and stems at macro scale[6,7] (Figure 1). Revealing the mystery of chirality on different length scales is an intricate and challenging task and is crucial to tailor the properties of chiral functional materials. To date, however, what directs the chirality of the high-order assemblies is still poorly understood. Different mechanisms have been proposed to interpret the chirality problem. In some cases, the chiral morphology of nanotubes or nanobelts results from faster growth on one side of the growth plane;[1,2] namely, the kinetic effect leads to the high-order chirality. In other cases, some previous reports revealed that the macroscopic chirality is determined by the chirality at the lower structural level due to non-parallel packing of neighboring motifs, namely, the bulk effect.[8] As a result, the enantiomeric compound possesses the opposite chirality at higher structural levels.[4,9−12] However, there are more and more experimental observations on twisting chirality of polymer lamellar crystals that cannot be interpreted by the above physical mechanisms. For instance, the lamellar crystals of poly(*R*-3-hydroxybutyrate) and its copolymers crystallized from melt twist in a defined sense,[13] while those crystallized from dilute solution are flat[14] although they have the same chirality in the lower structural levels. In addition, we found that poly(*R*-3-hydroxyvalerate) lamellae demonstrated right-handed and left-handed chirality when twisted along the *b* and *a* axis, respectively.[15] Unbalanced surface stresses have been proposed as a driving force of twisting and bending of polymer lamellar crystals,[16,17] where the surface stresses originate from the different degrees of overcrowding on the opposite fold surfaces. However, the quantitative relation between the surface stresses and the twisting chirality of lamellar crystals of chiral polymers is still unclear.

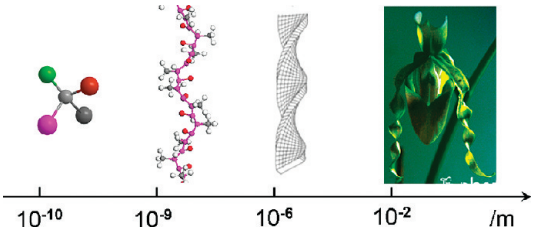

Figure 1. Expression of chirality at different structural levels. From left to right: chirality at the molecular level, chirality of chain stem, chirality of lamellar crystal,[4] and chirality of the flower petals of *Paphiopedilum dianthum*.[7]

In this article, the chiral growth habits of lamellar crystals of microbially synthesized nonracemic chiral poly(hydroxyalkanoate)s (PHAs) are investigated. Via copolymerization with other monomers or blending with other PHAs, we can tune the chiral twist sense of the lamellar crystals without changing the chirality at the lower structural levels. Asymmetric growth habits of the chiral polyesters were reported as well. A continuum mechanics model accounting for the effects of anisotropic surface stresses is proposed to interpret the observed twist sense inversion. Via mechanics simulation, we attempt to answer the following questions: How do the surface stresses affect the chiral sense of lamellar curvature (bending and twisting) in chiral polymers? What is the relationship between bending direction and twisting chirality of lamellar crystals? How does the crystallization temperature affect the magnitude of the surface stresses?

*Corresponding authors. E-mail: jun-xu@tsinghua.edu.cn (J.X.); fengxq@tsinghua.edu.cn (X.-Q.F.).

 Published on Web 06/15/2010

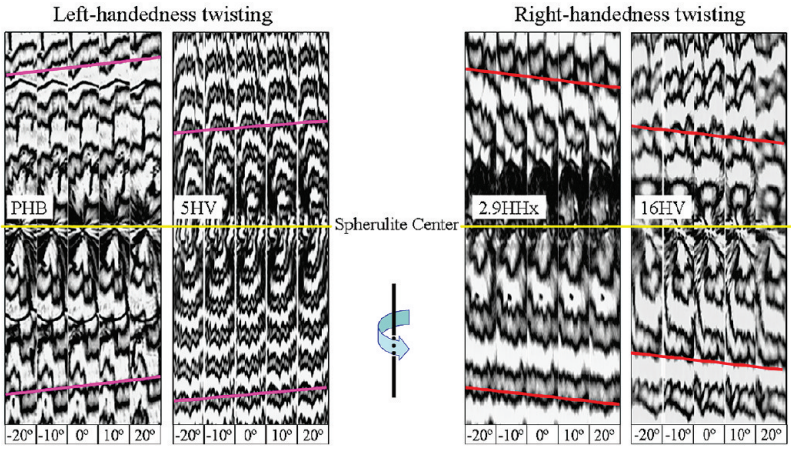

Figure 2. Lamellar twisting handedness in the spherulites of PHB, PHB with 5 mol % HV comonomers, 2.9 mol % HHx comonomers, and 16 mol % HV comonomers. The isothermal crystallization temperature of the samples was 80 °C.

Experimental Section

Materials. Poly(*R*-3-hydroxybutyrate-*co*-*R*-3-hydroxyhexanoate) random copolymer (PHBHHx) with 4.6 and 17 mol % 3-hydroxyhexanoate (HHx) content was fractionated according to Inoue's method[18,19] from the as-produced copolymer biosynthesized by *Aeromonas hydrophila* 4AK4.[20]

Poly(*R*-3-hydroxybutyrate-*co*-*R*-3-hydroxyvalerate) copolymers (PHBV) were synthesized in *Azotobacter vinelandii* UWD from sucrose and valeric acid.

Preparation and Characterization of the Samples. The sample for AFM observation was spin-coated onto freshly cleaved mica from 0.5% (w/v) chloroform solution, and then sample was kept in vacuum at room temperature for overnight to remove the residual solvent. Thereafter, it was mounted on the thermal stage in a Nanoscope III MultiMode AFM (Digital Instruments, now Veeco) for real-time observation of the lamellar growth at 75 °C. TESP tips with a resonance frequency of ~300 kHz and a spring constant of about 30 N/m were used. Tapping mode was applied to obtain both the height and phase images.

To investigate the effect of HHx comonomer content on lamellar twisting, the blends of PHB and PHBHHx-4.6 with different molar ratios were prepared via casting from 1% (w/v) chloroform solution and further evaporation of the solvent in vacuum.

The lamellar twist handedness in the spherulites was determined under a polarized optical microscope via tilting the sample stage.[9,10,15,21] A twisted lamella rotating in the sense of its own twist leads to a descent of the corresponding extinction rings. For example, right-handed rotation of right-handed twisting lamella leads to extinction bands moving toward the spherulite center, and right-handed rotation of left-handed twisting lamella leads to the extinction bands moving away from the spherulite center.

Results

It has been reported that the lamellar crystals in poly(*R*-3-hydroxybutyrate) (PHB) banded spherulite twist in left-handed sense,[10] while those in poly(*R*-3-hydroxybutyrate-*co*-17 mol %-*R*-3-hydroxyhexanoate) random copolymer (PHBHHx-17) twist in right-handed sense.[22] So we wonder how about the twisting chirality of lamellar crystals in PHBV and PHBHHx copolymers with various comonomer content. We have PHBV copolymers with different 3-hydroxyvalerate (HV) content at hand. For PHBHHx copolymers with 4.6, 8, 12, and 17 mol % HHx content, the lamellae all twist in right-handed sense. Since we do not have PHBHHx copolymers with HHx content ranging from 0 to 4.6%, we blend PHB with PHBHHx-4.6 with various blending ratios to get the blends with HHx content in the desired range. By varying the copolymer composition or blending ratio, we change the twist chirality of the lamellar crystals of microbially synthesized chiral PHAs. In PHB, the lamellar twist is left-handed, while in PHBV random copolymers and PHB/PHBHHx-4.6 blends the lamellar twist sense inverts to be right-handed with the increase in HV and HHx comonomer content (Figures 2 and 3). This novel observation indicates that one may tune the chiral sense of the polymer lamellae while keeping the molecular chirality unchanged. It also demonstrates that the chirality of lamellar twisting is not uniquely determined by molecular chirality. The reason why the band spacing in Figure 3a,b shows different trends with increase of the comonomer content will be interpreted in the following discussion section.

In PHBV copolymers, HV monomers exist in both the crystalline lamellar core and the amorphous fold surfaces,[23] whereas in PHBHHx copolymer, HHx monomers are excluded from the crystalline lamellar core and enriched mainly on the amorphous fold surfaces.[24] We did not observe component segregation in the blends of PHB and PHBHHx-4.6, as is in agreement with Feng et al.'s report that PHBHHx with HHx content less than 20 mol % is miscible with PHB in the amorphous phase.[25] Wide-angle X-ray diffraction reveals that PHBHHx and PHB have the same crystalline lattice,[24] so the helical chain stems in them are both of left-handed sense.[26,27] Consequently, the chirality inversion in PHB copolymers with the same monomer and the helical chain stem chirality cannot be interpreted by the existing models based on the crystalline core difference and should be attributed to the surface stresses effect. For PHBV, the critical comonomer content leading to the inversion of lamellar twisting chirality is about 15 mol % HV, while for PHB/PHBHHx-4.6 blends, it is only about 2.5 mol % HHx. The difference could be attributed to the larger volume of HHx comonomer unit and the fact that not all HV units were precluded into the fold surfaces.

To gain further insight in the physical mechanisms of lamellar twisting, we investigated the chiral growth habits of the lamellar crystals of a poly(*R*-3-hydroxybutyrate-*co*-17 mol %-*R*-3-hydroxyhexanoate) (PHBHHx-17) copolymer in thin films via real-time atomic force microscopy. The very low growth rate (~5 nm/s) and the occurrence of lamellar twisting in a wide range of temperature allow clear observation of the growth process of individual lamella.[22] In the film with thickness about 10 μm, the lamellae assume right-handed twist (Figure 4a), while in thinner film (thickness about 100 nm), the half lamellae show both counterclockwise bending and full lamellae right-handed twist (Figure 4b). With further increasing the crystallization temperature, sparsely separated twisting lamella can be observed (Figure 4c). When blended with amorphous atactic poly(*R*,*S*-3-hydroxybutyrate) (aPHB), the edge-on lamellae of PHBHHx-17 display more prominent lamellar bending toward the counterclockwise direction (Figure 4d).

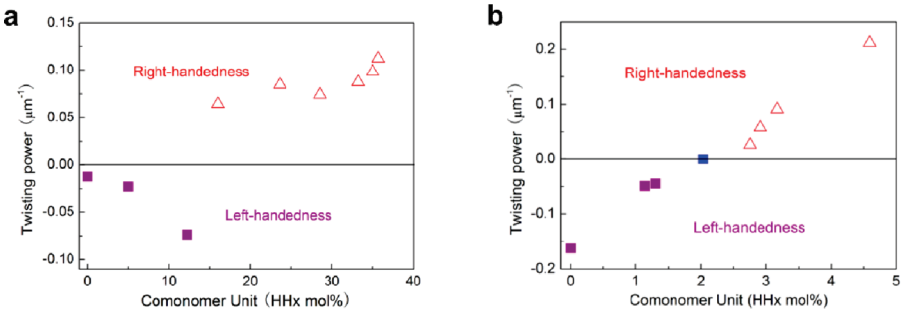

Figure 3. Inversion of twisting handedness of the polymer lamellae. (a) PHBV random copolymers crystallized at 85 °C. (b) Blends of PHB with PHBHHx-4.6 crystallized at 70 °C. The comonomer content is adjusted via changing the blend ratio of the two components, which are miscible in the melt and will not phase separate during crystallization. The twisting power is the reciprocal of the twisting pitch. Right-handed twisting is considered as positive and left-handed twisting negative.

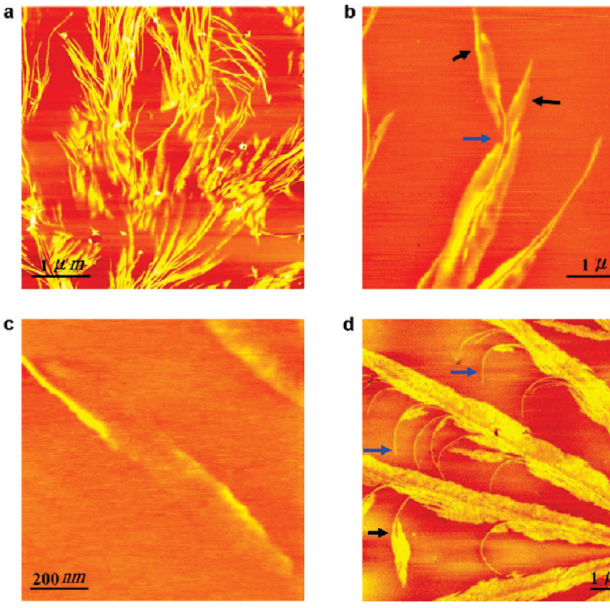

Figure 4. Chiral growth habits of lamellar crystals in PHBHHx-17 thin film. (a) Right-handed twisting full lamellae in the 10 μm thick film. (b) Simultaneous counterclockwise bending and right-handed twisting of the half lamellae crystallized in a thin film with thickness around 100 nm at 75 °C. (c) An individual twisting lamella crystallized at 85 °C. (d) More apparent bending and twisting of half PHBHHx-17 lamellae in its blended melt with atactic PHB. The blue and black arrows indicate lamellar bending and twisting, respectively.

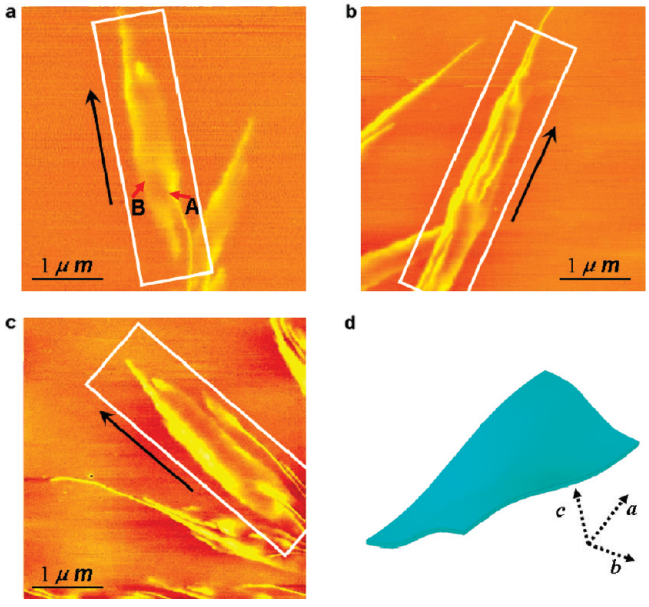

Figure 5. AFM images and the scheme showing the curvature of the lamella crystallized at 75 °C. The *a*, *b*, and *c* axis is also the there 2_1 helix axes of the lamella. The arrows indicate the radial growth direction (*a* axis) and the rectangular frames indicate the lamella with complicated curvature, which shows *S* and anti-*S* profile when viewed against the radial growth direction and the tangential direction, respectively. Namely, it is a double twisted lamella.

The lamellae of PHBHHx-17 appear S-shape curvature along both the radial (*a* axis) and the tangential growth direction (*b* axis) (Figure 5); however, the radii of curvature along the two orthogonal directions are not equal, implying that the surface stresses along the two directions are different in magnitude; namely, the surface stresses are anisotropic. The appearance of the lamella is the coupled curvature of bending, scrolling, and twisting, which makes it difficult to determine the twisting pitch from the orientation change of the lamella via AFM observation. For instance, in Figure 4a,c, lamellar twist occurs smoothly along the radial growth direction. At the same time, along the tangential direction, the lamella scrolls during widening. In Figure 5a, the edge-on lamella (very narrow due to the confinement of the film thickness about 100 nm) connects to the central line of the flat-on lamella at point A. At point A, the lamellar surface is tilted due to smooth twisting, but at point B, it is flat-on due to lamellar scrolling along the tangential width direction. As a consequence, if we judge the orientation change from the edge-on lamella and point B, we will get the wrong perception that the lamellar orientation changes abruptly, which is the reason why abrupt change of lamellar orientation was asserted from the results on the mature banded spherulites in previous report.[28] The explanation can also solve the point arised by Fromsdorf et al.[29] They argued that for our PHBHHx-17 sample the band spacing determined from POM was around 3−5 μm, but from the AFM image, the twisting pitch was only around several hundreds of nanometers. In fact, from Figure 4b, the twisting pitch is around 3−5 μm, which agrees with the band spacing determined from the POM image.

Furthermore, asymmetric branching of the flat-on lamellae at one preferred side, the counterclockwise side, was observed in the thin film of PHBHHx-17/aPHB blend (Figure 4d). The real-time bending and twisting process of the lamellae observed under AFM is demonstrated in Figure 6. It is shown that the flat-on branches are formed from twisting growth of the counterclockwise bending edge-on lamellae linked to the flat-on mother lamella (Figure 6a−d). Backward growth of the flat-on branches finally hides the interconnected edge-on lamellae (Figure 6e,f). In Figure 6 the two sectors of the flat-on lamellae are asymmetric in shape. The clockwise sector (the right part of the growing up lamella) is wider than the counterclockwise sector due to the constraint of the edge-on lamellae at the clockwise side of the flat-on lamellae.

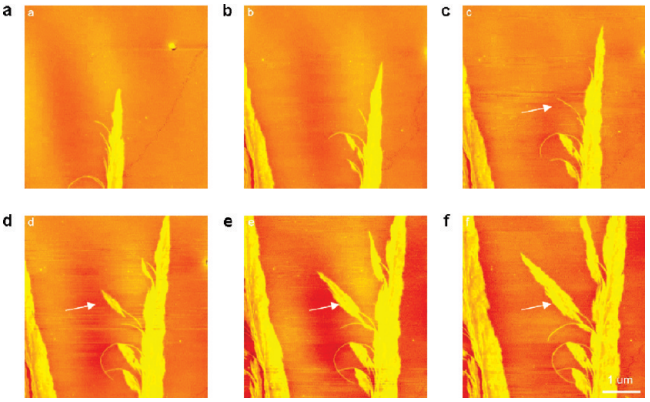

Figure 6. Real-time AFM phase images showing both counterclockwise bending and right-handed twisting of the half lamella in the thin film of PHBHHx-17 copolymer diluted with amorphous aPHB (the blending ratio is 60/40 in weight) crystallized at 75 °C.

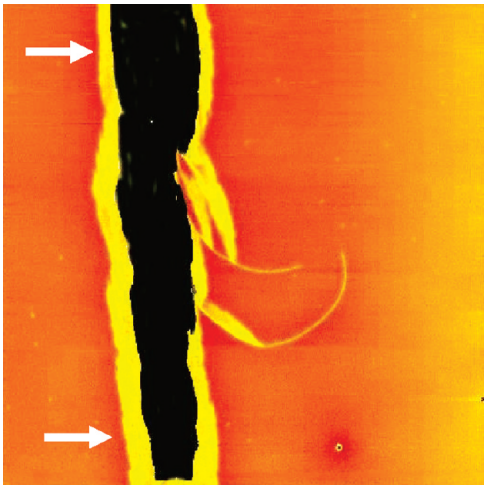

Figure 7. Same widening rate of the two halves of a flat-on lamella of PHBHHx-17 in the thin film blended with amorphous atactic PHB. The black profile represents the shape of the lamella 51 min ago.

However, the two sides of the flat-on lamellae have the same growth rate along the tangential direction, as revealed in Figure 7. If there is no constraint, the two halves of the flat-on lamellae are similar in shape, as presented in the rectangular frames in Figure 5. This is different from the case in polyethylene, where chain tilt leads to the asymmetric growth of the two halves of the flat-on lamella.[30] This implies that chain tilt is not the origin of the unbalanced surface stresses in the chiral polymers under study.

Recently, surface stresses were found to properly explain the chirality of lamellar bending and twisting of PLLA and PDLA lamellae.[9] Nonetheless, the edge-on lamellae of PDLA and PHBHHx-17 show the same (counterclockwise) bending direction, but they twist in the opposite handedness: the former shows left-handed twisting,[9] while the latter revealed right-handed twisting.[22] This discrepancy in the relationship between the bending direction and the twisting chirality cannot be interpreted by the existing theories; e.g., the bending of two halves at the opposite directions leads to twisting (the scheme proposed by Keith and Padden[16]). In the following, we will show that the discrepancy can still be interpreted in the frame of the model of anisotropic surface stresses.

Discussion

Effect of Surface Stresses on Lamellar Curvature. In what follows, we will attempt to interpret the twist sense inversion and the relationship between bending and twisting from the

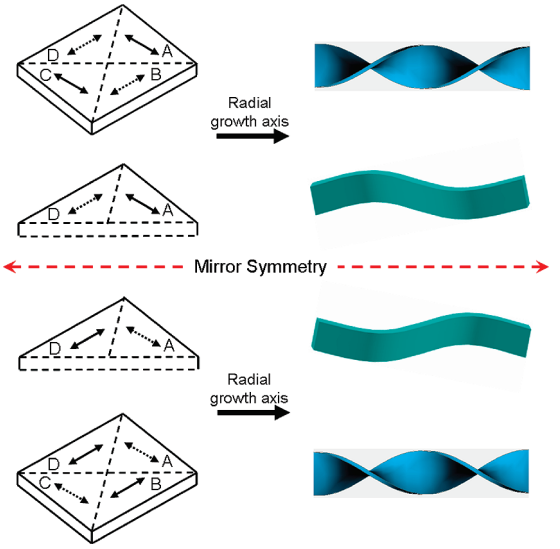

Figure 8. Scheme showing the distribution of the unbalanced surface stresses on fold surfaces of the lamellar crystals of chiral polymers in each sector and the resultant growth habbits. The surface stress distribution has a C_2 rotation axis along the radial growth direction. The molecular chirality affects the distribution of surface stresses and thus the macroscopic chirality of lamellar growth. Lamellar crystal of the enantiomeric chiral polymers has mirror symmetric distribution of the surface stresses, leading to the opposite twisting chirality and bending direction. The solid and dashed arrows indicate the surface stresses on the top and bottom surfaces, respectively.

viewpoint of unbalanced anisotropic surface stresses. During the growth process of lamellae from melt, the chain folds do not have sufficient time to achieve the equilibrium configuration with the minimal free energy before they entered into the crystalline state. As a result, surface stresses will appear on the fold surfaces, forcing the lamella to twist and bend, leading to a decrease of the surface free energy and a simultaneous increase of the bulk elastic energy. Minimization of the total potential energy generates lamellar curving, which can occur in individual lamella without any additional constraint induced by, e.g., other interlocking lamellae. In other words, the lamellar bending and twisting are thermodynamically stable. This analysis differs from the previous proposition that the transient lamellar twist is fixed by the interlocking of neighboring lamellae[16] and is consistent with the experimental results on individually twisted polymer lamellae.[5,22] The distribution of surface stresses depends on the structures at the smaller length scales, e.g., molecular chirality (in case of chiral polymers), chain tilt (in case of nonchiral polymers), fold direction, chemical structure, and packing of the chemical groups on the fold surfaces; thus, the surface stress distribution bridges the morphology chirality at the macroscopic scale and the microscopic structures at smaller length scales, which provides us an opportunity to explore the intrinsic mechanisms of lamellar morphologies.

Measuring the distribution of surface stresses on polymer lamella is still a challenging issue. Nevertheless, molecular simulations on melt-crystallized polyethylene lamellae[31] and metal surfaces[32] reveal that the surface stresses are rather more than often anisotropic. From the deformation of lamellae, one can infer the twisting and bending moment in them. For PHA lamella growing from melt, there usually exist four sectors. In the top and bottom lamellar surfaces of the sectors, the surface stresses are anisotropic and unbalanced (Figure 8). PHBV and PHBHHx have crystalline structures similar to that of PHB. They have $P2_12_12_1$ crystal lattice symmetry with a, b, and c crystal axes parallel to the

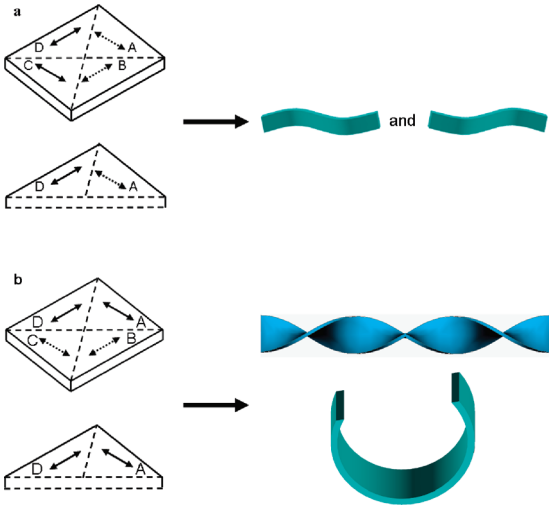

Figure 9. Two possible distributions of surface stresses in lamellae of nonchiral polymers, where exists a mirror plane.

three 2_1 screw axes.[24,26] The $P2_12_12_1$ symmetry means that if we turn the crystal 180° along each 2_1 screw axis and then shift a half pitch along the axis, the crystal will retain its original configuration. By analyzing the lamellar twisting and bending deformation, the surface stress distribution on PHA lamellae should have a C_2 rotation axis, as shown in Figure 8. Therefore, the full lamella will twist in a fixed sense along the two growth ends. For a half lamella or asymmetric lamella, there may exist only bending deformation or coupled twisting and bending deformation, depending on the magnitudes and directions of surface stresses on the sector surfaces. The enantiomeric chiral polymer will possess a mirror distribution of the surface stresses and thus the opposite twisting chirality and bending direction. Consequently, the mechanism based on surface stresses can interpret the opposite bending direction and twisting chirality of the enantiomeric polymers.

For nonchiral polymers, the surface stress distribution will be different from the above description due to the different symmetry of the crystalline structures, as shown in Figure 9. Figure 9a has a mirror plane parallel to the radial growth direction; namely, the net surface stresses on the bottom surface of sector A and B have the same magnitude but opposite directions. Their resultant rotation moment vanishes, and then the full lamella will not twist, which gives the reason why there is not twist in polyethylene hollow-pyramid type lamellae. The half lamella will bend clockwise or counterclockwise, with the same probability. In Figure 9b, there is a mirror plane along the tangential direction and a C_2 rotation axis along the radial direction, and correspondingly, a full lamella will twist in left- and right-handed sense and a half lamella will bend clockwise and counterclockwise along the two growth ends, respectively. Figure 9b corresponds to bending and twisting of chain-tilt lamellae of nonchiral polymers.

Relaxation of Surface Stresses Behind the Growth Tip or Surface Stresses at the Growth Tip Lead to Lamellar Curvature? Either the relaxation of surface stresses behind the growth tip or surface stresses at the growth tip can lead to lamellar curvature. The tip of a growing lamella is softer than the behind region. For bending, it is difficult to distinguish the two mechanisms. But for lamellar twisting, the two cases will cause the opposite twisting chirality. For instance, if the surface stresses are slightly inclined to the radial direction, e.g., the left half of the lamella in Figure 10a tends to bend

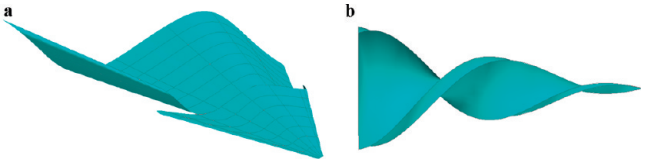

Figure 10. Different consequences of surface stresses relaxed at the behind part (a) or at the tip (b) of a growing lamella. It should be noted that the two mechanisms lead to the opposite apparent twist chirality, e.g., right-handed twist in (a) and left-handed twist in (b).

upward while the right half downward, the relaxation of surface stresses in the region behind the growth tip results in the apparent right-handed twisting. If the intensity of the surface stresses is larger than the yield stress of the lamella, plastic deformation will happen, leading to the nucleation of macro screw dislocations (Figure 10a). On the other hand, if surface stresses affect the growth tip, the left half part of the frontier bends upward while the right half bends downward, and thus the lamellar tip will twist in left-handed sense (Figure 10b). From the lamellar morphology shown in Figure 5, we conclude that in PHBHHx-17, it is the relaxation of surface stresses in the lamellar part behind the growth tip that leads to lamellar twisting. The relaxation of surface stresses has been observed in polyethylene tilted lamellae and proposed as the reason of lamellar twisting by Patel and Bassett.[33]

Mechanics Simulation of the Surface Stress Effect on Lamellar Bending and Twisting. To rationalize how the anisotropic surface stresses induce the lamellar twisting and bending and to model the above experimental results, we proposed a quantitative mechanics model based on the surface elasticity theory established by Gurtin et al.[34,35] This theory treats the surface as a two-dimensional membrane perfectly bonded to the bulk material without slipping being allowed. Such a treatment appears appropriate for the problem under study. Gurtin's theory of surface elasticity has been used to account for surface effects on the growth and physical behaviors of nanomaterials.[36,37] Compared to the previous analyses of twisting of nanobelts[3,38] and chiral liquid crystals,[8] our model is a substantial revision, where the surface layers with different mechanical properties arising from the core are taken into account and are treated as anisotropic rather than isotropic. The standpoint is reasonable for thin, nanosized crystalline or semicrystalline objects, which have a high surface/bulk ratio, so that the surface effect plays an important role in determining the curvature. In a previous report, Wang et al.[39] theoretically predicted that anisotropic surface stresses may induce twisting of nanowires, but they did not account for the coupling between bending and twisting, which is of crucial importance for the problem of current interest.

We now use the proposed model based on anisotropic surface stresses to interpret the inversion of twisting chirality with copolymerization/blending and the observed different bending directions of half lamella but with the same twisting chirality of full lamella. Simultaneous twisting and bending are considered in the present model. We consider a long polymer lamella of length l, width b, and thickness h with $l \gg b \gg h$, as shown in Figure 11a. For simplicity, the surface stresses on a sector are averaged on the whole sector. The azimuth angles of the principal axis of the surface stresses on the top and bottom lamellar surface of a lamella are indicated by θ^+ and θ^-, respectively. The effect of the surface stresses accounts to a virtual uniaxial tension or compression force F applied at the two ends of the lamella, which induces the longitudinal contraction or elongation as well as the

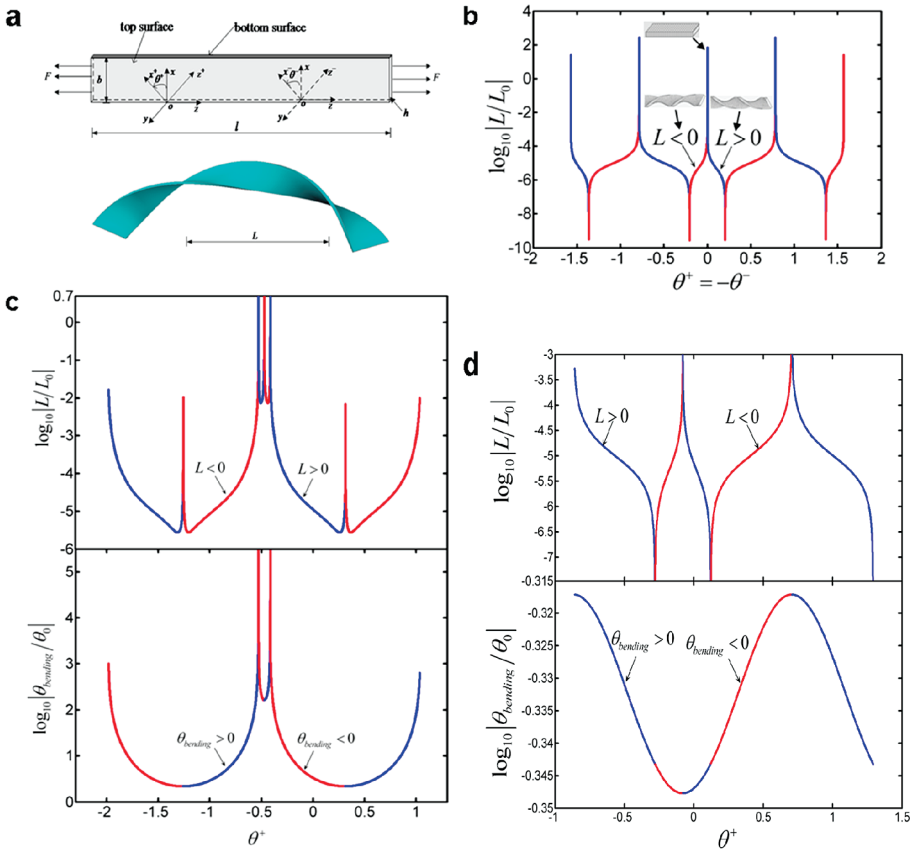

Figure 11. Scheme of the anisotropic surface stress model (a) and the resultant bending and twisting lamella (b−d). Variation of the half-twist pitch of a full lamella with (b) $\theta^- = -\theta^+$, (c) $\theta^- = -\theta^+ + 0.20\pi$, and (d) $\theta^- = -\theta^+ + 0.45\pi$ with respect to the azimuth angle θ^+ of the surface stresses. The blue and red curves stand for right- ($L > 0$) and left-handed ($L < 0$) twisting, respectively. (c) and (d) demonstrate the simulation result that the same bending direction may correlate to the opposite twisting chirality due to the different directions of the surface stresses. Here, we take $L_0 = 1$ m and $\theta_0 = 1°$.

bending and twisting deformation observed in our experiments (Figure 4b). For short, the detailed formulations of the model are given in the Appendix. Accounting for the axial deformation, twisting, and bending of both the surfaces and the crystallizing core, the total potential energy of the lamella can be expressed as

$$H = \frac{1}{2}(\lambda+2\mu)\varepsilon^2 hbl + \frac{1}{6}\mu\varphi^2 h^3 bl + \frac{1}{4}\varepsilon bl[2(c_{22}^+ + c_{22}^-)\varepsilon + (c_{23}^+ - c_{23}^-)\varphi h] + \frac{1}{4}\varphi hbl[2(c_{32}^+ - c_{32}^-)\varepsilon + (c_{33}^+ + c_{33}^-)\varphi h] + \frac{1}{32EI}h^2b^2l[2(c_{22}^+ - c_{22}^-)\varepsilon + (c_{23}^+ + c_{23}^-)\varphi h]^2 - F\varepsilon l \quad (1)$$

where $EI = Ebh^3/12$ is the bending stiffness of the crystallizing core and c_{ij}^+ and c_{ij}^- are the elastic constants of the top and bottom surfaces and vary with the azimuth angles θ^+ and θ^-, respectively (see Appendix). By minimizing the total potential energy H with respect to ε (tensile strain) and φ (twisting angle), the bending angle and twisting pitch of a curved lamella can be determined. As aforementioned, the twisting and bending deformations are induced by the unbalanced anisotropic surface stresses on the two surfaces of the lamella. Then the twisting pitch length and the bending angle are functions of the azimuth angles θ^+ and θ^- of surface stresses, as shown in eq A3 and eqs A7−A9 in the Appendix. In our model, therefore, the key parameters affecting the chirality of lamellar bending and twisting are the intensities and azimuth angles of the anisotropic surface stresses and the surface elasticity parameters.

We take a polymer lamella of thickness $h = 6$ nm and width $b = 100$ nm as an example. Its bulk elastic constants are taken as $\lambda = 8.714$ GPa and $\mu = 2.179$ GPa (or, equivalently, $E = 6.1$ GPa[38] and $\nu = 0.4$). The surface elastic constants have the following forms: $c_{1111}^{s\pm} = c_{2222}^{s\pm} = \lambda_s + \mu_s$, $c_{1122}^{s\pm} = c_{2211}^{s\pm} = \lambda_s - \mu_s$, and $c_{1212}^{s\pm}(A_0/2)(c_{1111}^s - c_{1122}^s)$, where $\lambda_s = 3.493\,87$ N/m and $\mu_s = -5.709\,15$ N/m.[36] The parameter A_0 indicates the degree of anisotropy of surface elasticity, and it may not be limited between 0 and 1 (isotropic, where no twist will occur[39]), as is different from that for bulk materials. In the computations, we take $A_0 = 0.25$ and $\sigma_0 = 30$ MPa.

Here we show the results of several representative simple examples, though more situations can be analyzed easily by this model. The first example assumes that the average surface stresses on the top and bottom surfaces have the same magnitude but different directions with $\theta^+ = -\theta^-$; namely, the surface stresses distribution has a C_2 rotation axis along the growth direction; namely, turning the lamella up−down will not change the surface stress distribution. The surface stresses in the symmetric full lamella of PHB, and its copolymers shown in Figure 8 are mechanically equivalent to this case. Our model predicts that the full lamellae with symmetric shape have no net bending (i.e., the central line is a straight line) but only helicoidal twisting providing that the surface stress distribution has a C_2 rotation axis along the growth direction. This theoretical result is consistent with our experimental observations (Figure 4a). The twisting pitch length L and the twisting chirality show sensitive dependence on the azimuth angle $\theta^\pm$ of the surface stresses, as shown in Figure 11b. This model accounts for the inversion of the twist handedness of PHB copolymer lamellae by

variation of the directions of the surface stresses on the two surfaces. Copolymerization changes the chemical structures on the fold surfaces and mediates the directions of the principal axes and the eccentricity of the surface stresses. For PHBV copolymers, θ^+ may decrease from $\pi/2$ to 0 with increase of HV comonomer content from 0 to 35 mol %, which tends to decrease the pitch of left-handed twisting, and then increase the pitch of right-handed twisting. At the same time, lamellar core thickness decreases sharply, tending to decrease the twisting pitch. Combination of the two effects results in the trend shown in Figure 3a. For PHB/PHBHHx-4.6 blends, θ^+ may increase from $\pi/2$ to π with increase of HHx content, tending to increase the pitch of left-handed twisting, and then decrease the pitch of right-handed twisting. Since the HHx content is low, the decrease of lamellar core thickness is slight, which has little effect on the twisting pitch. Consequently, the different trends in Figure 3a,b could be attributed to the different directions of surface stresses due to the different comonomers at the lamellar surface. In addition, the mechanical model predicts that for a given polymer chirality the chiral sense of lamellar twisting also depends on the growth axis along which twisting occurs. Lamellar crystals have opposite twist handedness if growth occurs along two orthogonal axes: *a* axis (with the azimuth angle of θ_a^+) and *b* axis ($\theta_b^+ = \pi/2 - \theta_a^+$). This is confirmed in the microbial poly(*R*-3-hydroxyvalerate) spherulite.[15]

In the second example, we assume that the average surface stresses on the top and bottom surface are still of the same magnitude but $\theta^+ \neq -\theta^-$. A PHA lamella consisted of two asymmetric halves is mechanically equivalent to this case. In this case, the lamella will bend and twist simultaneously. Variations of the twist pitch and bending curvature with θ^+ are demonstrated in Figure 11c,d. It is demonstrated that the twisting and bending of a half lamella are usually coupled for a certain chiral polymer, but the same bending direction of the half lamella in different polymers may correlate to the opposite twisting chirality of the full lamella due to the different direction of surface stresses (or the different surface elastic property), as is the case for poly(D-lactide) and PHBHHx-17. The full lamella consisting of two half lamellae will twist with the same handedness as the half lamella. Whether a full lamella bends or not relies on the symmetry of its shape. If its two halves have the same size, no bending will occur. However, the two halves of a lamella may have different sizes due to such reasons as possible asymmetric confinement in growth,[30] and in this case, bending and twisting may occur simultaneously, as revealed in Figure 4d.

As aforementioned, the azimuth angles θ^+ and θ^- depend on such factors as crystallographic structures, molecular chirality, and the direction of chain folding. For the material in this study, the anisotropy of surface stresses is mainly dictated by the chain folding structures on the top and bottom surfaces. Thus in our simulations, we determined the values of θ^+ and θ^- according to the features of chain folding. For PHB full crystal, if $\theta^+ = 0.13\pi$ and $\theta^- = -0.13\pi$, we obtain $\theta_{\text{bending}} = 0$ and $L = -3.198 \times 10^{-6}$ m with $\varepsilon = 0.0013$, where the negative value of L indicates left-handed twisting. While for the PHBHHx symmetric crystal, if $\theta^+ = 0.37\pi$, $\theta^- = -0.37\pi$, and the other parameters remain the same, the bending angle $\theta_{\text{bending}} = 0$ and $L = 3.198 \times 10^{-6}$ m with $\varepsilon = 0.001\,34$. The positive value of L indicates right-handed twisting. The surface stresses on PHBHHx lamella can be obtained as $\sigma_{zz}^+ = 0.1049$ J/m^2 and $\sigma_{xx}^+ = -0.0956$ J/m^2, which are in a reasonable agreement with the results of simulations.[31] In addition, the obtained value of $\varepsilon = 0.001\,34$ is also within an appropriate range of typical polymer crystals, which will not lead to the defect structures or plastic deformation during the twisting deformation.[38]

For a PHBHHx half crystal with $\theta^+ = 0.47\pi$ and $\theta^- = -0.27\pi$, we can obtain $\theta_{\text{bending}} = -45°$, $L = 7.64 \times 10^{-6}$ m, and $\varepsilon = 0.001\,52$. The model shows that the half lamella will bend and twist simultaneously. Compared to the corresponding full lamella, the twisting deformation is smaller.

In the third example, we assume that the average surface stresses on the top and bottom surfaces have different magnitudes but the same direction. The half lamella schemed in Figure 8 accords with this case. Due to the unbalanced surface stresses, the half lamella will bend when $\theta^+ = \theta^- = 0$, scroll when $\theta^+ = \theta^- = \pi/2$, or helically twist when $\theta^+ = \theta^- \neq 0$ or $\pi/2$, depending on the direction of the surface stresses. In more other cases, the surface stresses may create different geometric morphologies of the lamellae but are omitted here for short.

In our model, the surface stresses exist on the total lamellar surfaces, though they may have different directions and amplitudes on top and bottom surface in different sectors. The lamellar thickness considerably affects the lamellar curvature. This is different from the effect of bulk stress, where twisting pitch varies with crystal width.[3] In addition, recently, Shtukenberg et al.[40] report crystal twisting and untwisting resulting from heterometry of internal stress. In our opinion, the heterometric internal stress is similar to the surface stresses, both existing on the outside layer of the crystal. The difference of them is that the fraction of outside layer with internal stress reported by Shtukenberg et al. decreases with increase of the size of crystal cross section (both width and thickness), while the fraction of layer with surface stress reported by us is constant with increase of crystal cross section (only width increases with constant thickness). Consequently, the crystal with heterometric internal stress can untwist, while that with surface stresses cannot, as revealed in the aforementioned part.

Dependence of Surface Stress on Supercooling. From the bending curvature of half lamella, the magnitude of surface stress can be estimated. According to Stoney's equation[41,42]

$$\varphi = \frac{Et^2}{6R(1-\nu)} \tag{2}$$

where φ is the applied surface stress (N/m), E the Young's modulus of the lamella (N/m^2), t the thickness of the lamella (m), R the radius of bending curvature of the lamella (m), and ν Poisson's ratio. From eq 2, the surface stress of PLA lamellae crystallized at 120 °C is estimated to about 0.4 N/m ($E = 6$ GPa, $R = 2$ μm, $t = 20$ nm, $\nu = 0.5$) along the growth direction. It should be noted that the above stress is the net differential stress between the bottom and up fold surface, which is of the same order as that in the melt-crystallized PE lamellae simulated by Hütter et al. (-0.27 and -0.4 J/m^2 in the two normal directions).[31] In addition, Rutledge's result confirms the anisotropy of the surface stresses in the melt crystallized polymer lamellae.

Combining the temperature dependence of curvature radius of bending (fitted with the data adopted from Figure 10 in the literature[22]) and variance of the lamellar thickness in PHBHHx-17 with supercooling:

$$R \propto \Delta T^{-3.6} \tag{3}$$

$$t \propto \Delta T^{-1} \tag{4}$$

We can obtain the temperature dependence of the surface stress:

$$\varphi \propto \Delta T^{1.6} \tag{5}$$

Equation 5 indicates that the surface stress is proportional to the supercooling. It can successfully explain why solution-crystallized PHA single crystals are usually flat while those crystallized from melt are twisted, where the supercooling is different at the two cases.

Conclusions

The twisting chirality of polyhydroxyalkanoate lamellae with chiral center in the backbone is observed to invert from left-handed to right-handed with copolymerization and blending, which is successfully interpreted by the proposed mechanical model based on anisotropic surface stresses. Theoretical simulations show that the distribution of anisotropic surface stresses has considerable influence on the morphologies of lamellar crystals. Alteration of the direction of surface stresses may change the twisting chirality. In addition, the shape of the lamella affects lamellar curvature; e.g., half lamella and full lamella may show different curving habits. The proposed mechanism fills the gap between the molecular chirality and the chiral habits of the high-order assemblies and reveals the complexity of chirality. Furthermore, the surface stresses vary with supercooling when crystallized from melt. The larger the supercooling, the larger surface stresses. In future work, molecular simulations and microscopic mechanical experiments will be performed in an attempt to determine the exact values of the surface stresses and the surface elasticity properties as functions of such factors as molecular chirality, fold surface structure, crystallization dynamics, etc. The method and results reported here are not limited to polymers and also applicable to various fields, such as chiral liquid crystals, biofilms and biomembranes, and micro/nano-sized soft matter belts and tubes.

Acknowledgment. This work was supported by the National Natural Science Foundation of China (Grants 20504019, 50673050, 10972121, 10732050, 10802041, and 20974060) and 973 Project (2010CB631005). J. Xu is grateful to Professor Marek Kowalczuk for providing atactic poly(*R,S*-3-hydroxybutyrate). We are indebted to Prof. Bernard Lotz for intensive discussions on the manuscript.

Appendix. Model of the Curved Lamellar Morphology

We consider a long polymer lamella of width b, thickness h, and length l with $l \gg b \gg h$, as shown in Figure 11a. The azimuth angles of the principal axis of the surface stresses on the top and bottom lamellar surface are indicated by θ^+ and θ^-, respectively. The effect of the surface stresses equals to the consequence of a virtual uniaxial tension or compression force F applied at the two ends of the nanolamella.

The surface elastic constitutive relations can be written in these two local coordinate systems as

$$\sigma_{\alpha\beta}^{s\pm} = c_{\alpha\beta\gamma\delta}^{s\pm}\varepsilon_{\gamma\delta}^{s\pm} \tag{A1}$$

where $\sigma_{\alpha\beta}^{s}$ denote the surface stresses, $\varepsilon_{\gamma\delta}^{s}$ the surface strains, and $c_{\alpha\beta\gamma\delta}^{s\pm}$ the surface elastic constants. Throughout the paper, Einstein's summation convention is adopted for all repeated Latin indices over (1, 2, 3) and Greek indices over (1, 2). The superscript "$s\pm$" denotes the physical quantities on the top and bottom surfaces, respectively.

The surface stresses in the global coordinate system (o-xz) $\sigma_{xx}^{\pm}$, $\sigma_{zz}^{\pm}$, and $\tau_{xz}^{\pm}$ can be obtained via the coordinate transformation as

$$\begin{aligned}\sigma_{xx}^{\pm} &= c_{11}^{\pm}\varepsilon_{xx}^{\pm} + c_{12}^{\pm}\varepsilon_{zz}^{\pm} + c_{13}^{\pm}\varepsilon_{xz}^{\pm}\\ \sigma_{zz}^{\pm} &= c_{21}^{\pm}\varepsilon_{xx}^{\pm} + c_{22}^{\pm}\varepsilon_{zz}^{\pm} + c_{23}^{\pm}\varepsilon_{xz}^{\pm}\\ \tau_{xz}^{\pm} &= c_{31}^{\pm}\varepsilon_{xx}^{\pm} + c_{32}^{\pm}\varepsilon_{zz}^{\pm} + c_{33}^{\pm}\varepsilon_{xz}^{\pm}\end{aligned} \tag{A2}$$

where $\varepsilon_{xx}^{\pm}$, $\varepsilon_{zz}^{\pm}$, and $\varepsilon_{xz}^{\pm}$ are the surface strain and $c_{ij}^{\pm}$ $(i,j = 1-3)$ denotes the surface elastic coefficients on the two surfaces. $c_{ij}^{\pm}$ in eq A2 can be expressed as

$$\begin{aligned}c_{11}^{\pm} &= c_{1111}^{s\pm}\cos^4\theta^{\pm} + 2(c_{1122}^{s\pm} + 2c_{1212}^{s\pm})\cos^2\theta^{\pm}\sin^2\theta^{\pm} + c_{2222}^{s\pm}\sin^4\theta^{\pm}\\ c_{12}^{\pm} &= (c_{1111}^{s\pm} + c_{2222}^{s\pm} - 4c_{1212}^{s\pm})\cos^2\theta^{\pm}\sin^2\theta^{\pm} + c_{1122}^{s\pm}(\cos^4\theta^{\pm} + \sin^4\theta^{\pm})\\ c_{22}^{\pm} &= c_{1111}^{s\pm}\sin^4\theta^{\pm} + 2(c_{1122}^{s\pm} + 2c_{1212}^{s\pm})\cos^2\theta^{\pm}\sin^2\theta^{\pm} + c_{2222}^{s\pm}\cos^4\theta^{\pm}\\ c_{31}^{\pm} &= (-c_{1111}^{s\pm} + c_{1122}^{s\pm} + 2c_{1212}^{s\pm})\cos^3\theta^{\pm}\sin\theta^{\pm}\\ &\quad + (-c_{1122}^{s\pm} + c_{2222}^{s\pm} - 2c_{1212}^{s\pm})\cos\theta^{\pm}\sin^3\theta^{\pm}\\ c_{32}^{\pm} &= (-c_{1111}^{s\pm} + c_{1122}^{s\pm} + 2c_{1212}^{s\pm})\cos\theta^{\pm}\sin^3\theta^{\pm}\\ &\quad + (-c_{1122}^{s\pm} + c_{2222}^{s\pm} - 2c_{1212}^{s\pm})\cos^3\theta^{\pm}\sin\theta^{\pm}\\ c_{33}^{\pm} &= \frac{1}{2}(c_{1111}^{s\pm} + c_{2222}^{s\pm} - 2c_{1122}^{s\pm})\sin^2 2\theta^{\pm} + 2c_{1212}^{s\pm}\cos^2 2\theta^{\pm}\\ c_{13}^{\pm} &= 2c_{31}^{\pm}\\ c_{23}^{\pm} &= 2c_{32}^{\pm}\end{aligned} \tag{A3}$$

Let ε denote the strain of the lamella in the length direction and φ the rotational angle of the lamellae per unit length with respect to the z-axis. From the theory of elastic beams and surface elasticity theory, the surface stresses are related to ε and φ via the relation

$$\sigma_{zz}^{+} = c_{22}^{+}\varepsilon + \frac{1}{2}c_{23}^{+}\varphi h, \quad \tau_{xz}^{+} = c_{32}^{+}\varepsilon + \frac{1}{2}c_{33}^{+}\varphi h \tag{A4}$$

$$\sigma_{zz}^{-} = c_{22}^{-}\varepsilon - \frac{1}{2}c_{23}^{-}\varphi h, \quad \tau_{xz}^{-} = c_{32}^{-}\varepsilon - \frac{1}{2}c_{33}^{-}\varphi h \tag{A5}$$

Considering the axial deformation, twisting and bending of both the surfaces and the crystallizing core, the total potential energy of the lamella can be expressed as

$$\begin{aligned}H &= \frac{1}{2}(\lambda + 2\mu)\varepsilon^2 hbl + \frac{1}{6}\mu\varphi^2 h^3 bl + \frac{1}{4}\varepsilon bl[2(c_{22}^{+} + c_{22}^{-})\varepsilon\\ &\quad + (c_{23}^{+} - c_{23}^{-})\varphi h] + \frac{1}{4}\varphi hbl[2(c_{32}^{+} - c_{32}^{-})\varepsilon + (c_{33}^{+} + c_{33}^{-})\varphi h]\\ &\quad + \frac{1}{32EI}h^2 b^2 l[2(c_{22}^{+} - c_{22}^{-})\varepsilon + (c_{23}^{+} + c_{23}^{-})\varphi h]^2 - F\varepsilon l\end{aligned} \tag{A6}$$

where $EI = Ebh^3/12$ is the bending stiffness of the crystallizing core and c_{ij}^{+} and c_{ij}^{-} are the elastic constants of the top and bottom surface, respectively. They are obtained as $c_{1111}^{s\pm} = c_{2222}^{s\pm} = \lambda_s + \mu_s$, $c_{1122}^{s\pm} = c_{2211}^{s\pm} = \lambda_s - \mu_s$, and $c_{1212}^{s\pm} = A_0(c_{1111}^{s} - c_{1122}^{s})/2$. A_0 is a parameter describing the anisotropy degree of surface elasticity. A_0 may not lie between 0 (completely anisotropic) and 1 (isotropic). If A_0 equals 1, namely the surfaces are isotropic, no twist will occur.[33] By minimizing the total potential energy H with respect to ε and φ, the bending angle and twisting pitch of a curved lamella can be obtained.

Denote the half twist pitch length as L (Figure 11a). By minimizing the total potential energy H with respect to ε and

φ, one has

$$\varphi = \frac{\sigma_0}{AQ+B}, \quad L = \frac{\pi}{\sigma_0}(AQ+B) \tag{A7}$$

where $\sigma_0 = F/(bh)$ and

$$\begin{aligned} A &= \lambda + 2\mu + \frac{1}{h}(c_{22}^{+} + c_{22}^{-}) + \frac{3}{Eh^2}(c_{22}^{+} - c_{22}^{-})^2 \\ B &= (c_{32}^{+} - c_{32}^{-})\left[1 + \frac{3}{Eh}(c_{22}^{+} - c_{22}^{-})\right] \\ Q &= -\frac{\frac{1}{3}\mu h^2 + \frac{h}{2}(c_{33}^{+} + c_{33}^{-}) + \frac{3}{E}(c_{32}^{+} + c_{32}^{-})^2}{\frac{3}{Eh}(c_{22}^{+} - c_{22}^{-})(c_{32}^{+} + c_{32}^{-}) + c_{32}^{+} - c_{32}^{-}} \end{aligned} \tag{A8}$$

Then the bending angle θ_{bending} within the half twist pitch length L is obtained as

$$\theta_{\text{bending}} = \frac{1}{2EI}\left[(c_{22}^{+} - c_{22}^{-})\varepsilon + \frac{1}{2}(c_{23}^{+} + c_{23}^{-})\varphi h\right] hbL \tag{A9}$$

Using eqs A8 and A9, one can determine the magnitude and sense of lamellar bending and twisting, which vary with the azimuth angles θ^{+} and θ^{-} of surface stresses.

References and Notes

(1) Yu, S.-H.; Cölfen, H.; Tauer, K.; Antonietti, M. *Nature Mater.* **2005**, *4*, 51–55.
(2) Garcia-Ruiz, J. M.; Melero-Garcia, E.; Hyde, S T. *Science* **2009**, *323*, 362–365.
(3) Oda, R.; Huc, I.; Candau, S. J.; MacKintosh, F. C. *Nature* **1999**, *399*, 566–569.
(4) Lotz, B.; Gonthier-Vassal, A.; Brack, A.; Magoshi, J. *J. Mol. Biol.* **1982**, *156*, 345–357.
(5) Li, C. Y.; Cheng, S. Z. D.; Ge, J. J.; Bai, F.; Zhang, J. Z.; Mann, I. K.; Harris, F. W.; Chien, L.-C.; Yan, D.; He, T.; Lotz, B. *Phys. Rev. Lett.* **1999**, *83*, 4558–4561.
(6) Schulgasser, K.; Witztum, A. *J. Theor. Biol.* **2004**, *230*, 281–288.
(7) The *Paphiopedilum dianthum* picture is adopted from the website of http://www.huamu.com.cn/Html/xxnews/200912/11236.html.
(8) Emelyanenko, A. V. *Phys. Rev. E* **2003**, *67*, 031704.
(9) Maillard, D.; Prud'homme, R. E. *Macromolecules* **2008**, *41*, 1705–1712.
(10) Singfield, K. L.; Hobbs, J. K.; Keller, A. *J. Cryst. Growth* **1998**, *183*, 683–689.
(11) Saracovan, I.; Cox, J. K.; Revol, J.-F.; Manley, R.; St., J.; Brown, G. R. *Macromolecules* **1999**, *32*, 717–725.
(12) Singfield, K. L.; Klass, J. M.; Brown, G. R. *Macromolecules* **1995**, *28*, 8006–8015.
(13) Mitomo, H.; Barham, P. J.; Keller, A. *Polym. J.* **1987**, *19*, 1241–1253.
(14) Iwata, T.; Doi, Y.; Nakayama, S.-i.; Sasatsuki, H.; Teramachi, S. *Int. J. Biol. Macromol.* **1999**, *25*, 169–176.
(15) Ye, H. M.; Xu, J.; Guo, B. H.; Iwata, T. *Macromolecules* **2009**, *42*, 694–701.
(16) Keith, H. D; Padden, F. J., Jr. *Polymer* **1984**, *25*, 28–42.
(17) Lotz, B.; Cheng, S. Z. D. *Polymer* **2005**, *46*, 577–610.
(18) Watanabe, T.; Yong, H.; Fukuchi, T.; Inoue, Y. *Macromol. Biosci.* **2001**, *1*, 75–83.
(19) Feng, L. D.; Watanabe, T.; Wang, Y.; Kichise, T.; Fukuchi, T.; Chen, G. Q.; Doi, Y.; Inoue, Y. *Biomacromolecules* **2002**, *3*, 1071–1077.
(20) Chen, G. Q.; Zhang, G.; Park, S. J.; Lee, S. Y. *Appl. Microbiol. Biotechnol.* **2001**, *57*, 50–55.
(21) Keith, H. D.; Padden, F. J., Jr. *J. Polym. Sci.* **1959**, *39*, 101–123.
(22) Xu, J.; Guo, B. H.; Zhang, Z. M.; Zhou, J. J.; Jiang, Y.; Yan, S. K.; Li, L.; Wu, Q.; Chen, G. Q.; Schultz, J. M. *Macromolecules* **2004**, *37*, 4118–4123.
(23) Yoshie, N.; Saito, M.; Inoue, Y. *Macromolecules* **2001**, *34*, 8953–8960.
(24) Doi, Y.; Kitamura, S.; Abe, H. *Macromolecules* **1995**, *28*, 4822–4828.
(25) Feng, L. D.; Watanabe, T.; He, Y.; Wang, Y.; Kichise, T.; Fukuchi, T.; Chen, G. Q.; Doi, Y.; Inoue, Y. *Macromol. Biosci.* **2003**, *3*, 310–319.
(26) Cornibert, J.; Marchessault, R. H. *J. Mol. Biol.* **1972**, *71*, 735–756.
(27) Yokouchi, M.; Chatani, Y.; Tadokora, H.; Teranishi, K.; Tani, H. *Polymer* **1973**, *14*, 267–272.
(28) Crämer, K.; Lima, M. F. S.; Magonov, S. N.; Hellmann, E. H.; Jacobs, M.; Hellmann, G. P. *J. Mater. Sci.* **1998**, *33*, 2305–2312.
(29) Fromsdorf, A.; Woo, E. M.; Lee, L. T.; Chen, Y. F.; Forster, S. *Macromol. Rapid Commun.* **2008**, *29*, 1322–1328.
(30) Keith, H. D.; Padden, F. J., Jr; Lotz, B.; Wittmann, J. C. *Macromolecules* **1989**, *22*, 2230–2238.
(31) Hütter, M.; in't Veld, P. J.; Rutledge, G. C. *Polymer* **2006**, *47*, 5494–5504.
(32) Blanco-Rey, M.; Pratt, S. J.; Jenkins, S. J. *Phys. Rev. Lett.* **2009**, *102*, 026102.
(33) Patel, D.; Bassett, D. C. *Polymer* **2002**, *43*, 3795–3802.
(34) Gurtin, M. E.; Murdoch, A. I. *Arch. Ration. Mech. Anal.* **1975**, *57*, 291–323.
(35) Gurtin, M. E.; Weissmüller, J.; Larché, F. *Philos. Mag. A* **1998**, *78*, 1093–1109.
(36) Lu, P.; He, L. H.; Lee, H. P.; Lu, C. *Int. J. Solids Struct.* **2006**, *43*, 4631–4647.
(37) Wang, G. F.; Feng, X. Q.; Yu, S. W. *Europhys. Lett.* **2007**, *77*, 44002.
(38) Owen, A. G. *Polymer* **1997**, *38*, 3705–3708.
(39) Wang, J. S.; Feng, X. Q.; Wang, G. F.; Yu, S. W. *Appl. Phys. Lett.* **2008**, *92*, 191901.
(40) Shtukenberg, A. G.; Freudenthal, J.; Kahr, B. *J. Am. Chem. Soc.* **2010**, DOI: 10.1021/ja101491n.
(41) Stoney, G. G. *Proc. R. Soc. London A* **1909**, *82*, 172–175.
(42) Brenner, A.; Senderoff, S. *J. Res. Natl. Bur. Stand.* **1949**, *42*, 105.